

# Adatom capture by arrays of two-dimensional Ag islands on Ag(100)

M. C. Bartelt

*Sandia National Laboratories, Livermore, California 94550*

C. R. Stoldt, C. J. Jenks, and P. A. Thiel

*Department of Chemistry and Ames Laboratory, Iowa State University, Ames, Iowa 50011*

J. W. Evans

*Department of Mathematics and Ames Laboratory, Iowa State University, Ames, Iowa 50011*

(Received 12 August 1998)

We examine the capture of diffusing Ag adatoms by arrays of two-dimensional Ag islands subsequent to deposition on Ag(100) at room temperature. This is achieved by a combination of scanning tunneling microscopy experiments, kinetic Monte Carlo simulations, and diffusion equation analyses. The dependence of the capture rates on Ag-island size is shown to reflect larger island-free regions surrounding the larger islands, i.e., a strong correlation between island sizes and separations. This feature, and the influence of the local environment of the islands on capture, are elucidated by introducing suitable tessellations of the surface into “capture zones” for each island. We show that a Voronoi-type tessellation based on the distance from the island edges accurately reflects adatom capture. However, a tessellation exactly describing adatom capture is only obtained from a solution of the steady-state equation describing adatom deposition, diffusion, and capture by an array of islands distributed as in experiment. The stochastic nature of adatom capture is also quantified by analysis of the dependence on the deposition location of the probability for diffusing adatoms to be captured by a specific island. The experimental island size dependence of adatom capture is found to be entirely consistent with that obtained from a “canonical” model for the irreversible nucleation and growth of square islands.

[S0163-1829(99)14003-7]

## I. INTRODUCTION

The control of distributions of epitaxial islands on metal surfaces requires a basic understanding of the processes mediating their creation and relaxation. This includes a detailed description of the nucleation and growth of two-dimensional islands during deposition for a range of film growth conditions,<sup>1</sup> a key component of which is the capture of diffusing adatoms by individual islands. Such an understanding of capture also directly impacts on the development of rate-equation analyses for the evolution of populations of islands of various sizes,<sup>2,3</sup> as this relies on an appropriate specification of the island size dependence of the adatom capture rates.

In this paper, we present an analysis of the nature of diffusion-mediated capture of adatoms by near-square Ag islands during deposition on Ag(100) at room temperature. Here island formation and adatom capture are known to be effectively irreversible.<sup>4</sup> We find dramatic deviations from mean-field predictions. Larger islands have larger capture rates, reflecting the existence of larger empty regions surrounding such islands. We quantify these features for experimental Ag-island distributions, using both simulations of capture of randomly deposited and diffusing atoms, as well as deterministic diffusion equation analyses. Both a geometric interpretation and an analysis of the stochastic nature of adatom capture behavior are provided. Throughout, we compare the experimentally observed capture behavior with predictions from a “benchmark” simulation study of irreversible formation of near-square islands (where we can obtain essentially perfect statistics).

In Sec. II, we describe key features of the experimental setup, and of the observed Ag-island distributions. By way of background, a brief review of the basic concepts of adatom capture during deposition is provided in Sec. III. Then, in Sec. IV, we describe our Monte Carlo simulation procedure for analysis of atom capture in both experiment and in our “canonical” model. The behavior of the capture numbers, and their dependence on the size and local environment of the islands, are discussed in Secs. V and VI. A characterization of the stochastic nature of capture is provided in Sec. VII. In Sec. VIII, we compare the above results with capture behavior in recent experimental studies of the growth of two-dimensional Cu/Co islands on Ru(0001), and the growth of vacancy pits during etching of Si(001) surfaces with molecular oxygen. These studies underline the power of our analyses to characterize various aspects of capture. Finally, we summarize our main results, and outline ongoing studies, in Sec. IX.

## II. EXPERIMENTAL SETUP AND OBSERVATIONS OF ISLAND DISTRIBUTIONS

Silver was deposited from a resistively heated liquid-nitrogen-shrouded source onto an Ag(100) crystal held at room temperature in an ultrahigh-vacuum chamber (with a base pressure of  $6 \times 10^{-11} - 2 \times 10^{-10}$  Torr). The chamber is equipped with an Omicron room temperature scanning tunneling microscope (STM). STM images used in the capture analyses were obtained under low-resolution conditions, ap-

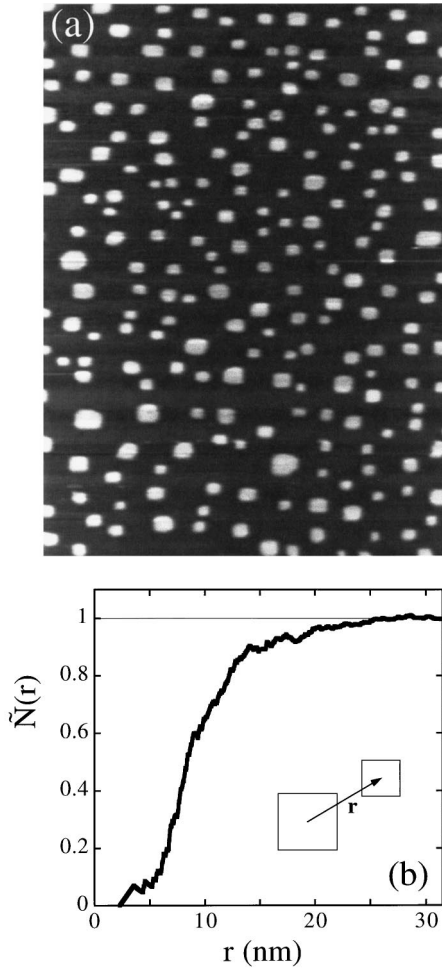


FIG. 1. (a)  $150 \times 200\text{-nm}^2$  STM image (taken 29 min after deposition) of a typical distribution of near-square islands of Ag on Ag(100), obtained at 295 K. The flux was  $F \approx 6.25 \times 10^{-2}$  ML/s, and  $\theta \approx 0.125$  ML. (b) Rotationally averaged and normalized pair-distribution function for island centers. Specifically,  $2\pi r N_{\text{av}} \tilde{N}(r) dr$  gives the expected number of islands with centers between a distance  $r$  and  $r + dr$  from that of an arbitrarily chosen island.

appropriate for minimizing tip effects, and for obtaining the number density, positions, and sizes of islands over broad terrace regions (typically about  $2000 \text{ \AA}$  wide). Uncertainty in such estimates of the positions and sizes of the islands comes mainly from uncertainty in determining the positions of the “frizzy” island edges in the STM images. The first images were typically obtained 15–45 min after deposition, so some loss of the smallest islands is likely to occur before STM imaging. Coverages, in ML, were determined directly from the STM images.

Figure 1(a) shows a typical distribution of two-dimensional Ag islands on Ag(100), obtained at room temperature, with a deposition flux  $F \approx 6.25 \times 10^{-2}$  ML/s. The coverage is  $\theta \approx 0.125$  ML, and the island density is  $N_{\text{av}} \approx 6.8 \times 10^{-3}/\text{nm}^2$ , so the average island separation is  $L_{\text{av}} \approx 12$  nm, and the average island size is  $s_{\text{av}} \approx 220$  atoms. The observed island shapes are essentially equilibrated, as expected, since edge diffusion is very fast compared to terrace diffusion.<sup>5</sup> Figure 1(b) shows the standard pair-distribution function  $\tilde{N}(r)$  for the separation of island centers,<sup>6,7</sup> with its characteristic strong depletion in the density of island pairs at

short separations  $r \ll L_{\text{av}}$ . This feature derives from a similar depletion in the adatom density near islands, which reduces the island nucleation probability near islands. Note that  $\tilde{N}(r)$  would be affected both by island diffusion (and subsequent coalescence) and by any Ostwald ripening of these islands after deposition.

Previous studies of the variation of the island density,  $N_{\text{av}}$ , with deposition flux  $F$ , have shown that island formation is effectively irreversible in this system at room temperature.<sup>4</sup> These studies have also shown that the diffusion of dimers and other small clusters does not significantly affect the island formation process. These observations motivate and justify our comparison below of adatom capture for experimental island distributions with capture for a canonical model of irreversible island formation.

### III. BASIC THEORETICAL CONCEPTS: ADATOM CAPTURE DURING DEPOSITION

Here we briefly review the key concepts in the theory of adatom capture by growing islands during deposition, and indicate the relationship between adatom capture rates and the island size distribution. The mean rate of capture of diffusing adatoms by islands of size  $s$  (which have a variety of local environments), defines the “capture number”  $\sigma_s$  for aggregation with islands of that size. In other words,  $\sigma_s$  gives the propensity for islands of size  $s$  to capture diffusing adatoms. More precisely, the rate of decrease in the number density,  $N_s$ , of islands of size  $s$ , due to aggregation with diffusing adatoms, of density  $N_1$  and hop rate  $h$ , equals  $R_{\text{agg}}(s) = h\sigma_s N_1 N_s$ . The total capture rate of adatoms by islands then satisfies  $R_{\text{agg}} = \sum_{s>1} R_{\text{agg}}(s) = h\sigma_{\text{av}} N_1 N_{\text{av}}$ , where  $N_{\text{av}} = \sum_{s>1} N_s$  is the average island density, and  $\sigma_{\text{av}} = \sum_{s>1} \sigma_s N_s / N_{\text{av}}$  is the average capture number for all islands.

Typically,  $\sigma_s$  have been analyzed at a mean-field (MF) level,<sup>8</sup> where the local environment of an island is assumed to be independent of its size and shape.<sup>9,10</sup> The MF  $\sigma_s$  were shown to scale like the island perimeter  $\sim s^{1/2}$  for large compact islands.<sup>9</sup> However, recent kinetic Monte Carlo simulation studies,<sup>11,12</sup> and experimental measurements of adatom capture for Cu/Co islands on Ru(0001),<sup>12</sup> showed that this MF form is *qualitatively* incorrect. The exact  $\sigma_s$  scales quasilinearly with large  $s$ , reflecting the feature that larger islands tend to have larger island-free regions surrounding them.<sup>11,12</sup> These same features are observed below in our study for Ag/Ag(100).

The dependence of  $\sigma_s$  on  $s$  is of particular importance as it controls the form of the island size distribution.<sup>11</sup> For the irreversible formation of immobile islands during deposition, relevant for Ag/Ag(100) epitaxy at room temperature, the number densities of diffusing adatoms,  $N_1$ , and islands of size  $s$ ,  $N_s$ , satisfy

$$dN_1/dt \approx F(1 - \theta) - 2R_{\text{agg}}(1) - \sum_{s>1} R_{\text{agg}}(s) \quad (1)$$

and

$$dN_{s>1}/dt \approx F(\Omega_{s-1}N_{s-1} - \Omega_s N_s) + R_{\text{agg}}(s-1) - R_{\text{agg}}(s). \quad (2)$$

Here  $t$  is time, and  $F$  is the deposition rate, so  $\theta = Ft = \sum_{s \geq 1} s N_s$  gives the coverage. The term  $F \Omega_s N_s$  describes ‘‘direct capture’’ by deposition on top of, or adjacent to, an island of size  $s$ . The terms  $R_{\text{agg}}()$  describe changes in the adatom and island populations due to aggregation of diffusing adatoms with islands of various sizes. These equations are often reduced by summing over  $s > 1$  to obtain

$$dN_1/dt \approx F(1 - \theta) - h \sigma_{\text{av}} N_1 N_{\text{av}}$$

and

$$dN_{\text{av}}/dt \approx h \sigma_1 (N_1)^2, \quad (3)$$

so in the steady-state regime one has  $N_1 \approx F(1 - \theta)/(h \sigma_{\text{av}} N_{\text{av}})$ .

For a large average island size,  $s_{\text{av}} \approx \theta/N_{\text{av}}$ , the solution of Eq. (2) has the form<sup>6,7</sup>

$$N_s \approx \theta (s_{\text{av}})^{-2} f(s/s_{\text{av}}), \quad (4)$$

where<sup>11</sup>

$$f(x) = f(0) \exp \left\{ \int_0^x dy [(2\bar{\omega} - 1) - C'(y)] / [C(y) - \bar{\omega}y] \right\}, \quad (5)$$

with  $' = d/dy$ ,  $\int_0^\infty f dy = \int_0^\infty y f dy = 1$ , and  $f(0) > 0$ . This analysis assumes that the capture numbers can be written in the scaling form

$$\sigma_s / \sigma_{\text{av}} \approx C(s/s_{\text{av}}), \quad (6)$$

where  $C$  and  $\bar{\omega} = d[\ln(s_{\text{av}})]/d[\ln(\theta)]$  are independent of  $\theta$ . Thus, the form of  $C$  (and the value of  $\bar{\omega}$ ) determine the form of  $f$ . In particular, the degree to which  $C(x)$  increases for large  $x$  controls whether or not  $f(x)$  diverges at some  $x$ .<sup>11</sup> Note that  $\bar{\omega} \approx 2/3$  for point islands, where  $N_{\text{av}} \sim \theta^{1/3}$ ,<sup>6</sup> but for islands of finite extent the enhanced tendency for saturation of  $N_{\text{av}}$  with  $\theta$  increases the effective value of  $\bar{\omega}$  toward unity.

#### IV. KINETIC MONTE CARLO SIMULATION ANALYSIS OF ADATOM CAPTURE

##### A. Adatom capture in a canonical model

In our canonical model,<sup>7</sup> atoms are deposited randomly, at rate  $F$  per site, on a square array of adsorption sites, and then hop to adjacent sites with rate  $h$ . Diffusing adatoms which meet other adatoms irreversibly nucleate new islands. Those which meet existing islands irreversibly aggregate with the islands. We enforce the near-square shape of the islands by always incorporating the aggregating atom at the kink site on the island edge. This mimics rapid diffusion at island edges, and efficient island shape equilibration, as applies to metal(100) homoepitaxy. Simulation results are presented for this model starting with an empty lattice, for appropriate  $h/F$  and fixed low  $\theta$ , choosing periodic boundary conditions for  $1000 \times 1000$  site (or larger) lattices.

##### B. Adatom capture in experiment

Analyses of adatom capture by experimental Ag-island arrays start instead with a distribution of near-square islands

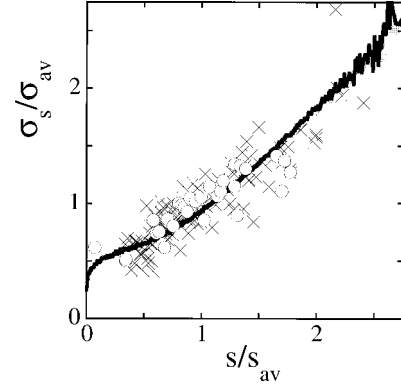


FIG. 2. Island size dependence of  $\sigma_s/\sigma_{\text{av}}$ , from simulations of irreversible nucleation and growth of square islands ( $\theta = 0.2$  ML; light gray line:  $h/F = 10^8$ ; dark gray line:  $h/F = 10^9$ ), and for island distributions matching those obtained on two Ag(100) single crystals:  $\times$ , 205 islands from Fig. 1(a);  $\circ$ , 81 islands from Fig. 5(a).

matching experiment. In fact, arrays formed in two separate experiments are used below. Here, we choose  $h/F$  consistent with the experimental flux,  $F \approx 0.01 - 0.1$  ML/s, and the values of  $h$  estimated previously from analysis of the flux and temperature dependence of the average island density.<sup>4</sup> At room temperature, one finds  $h \approx 3 \times 10^6$ /s. Data obtained for the Ag islands at the border of the STM images are discarded.

##### C. Technical details

To determine  $\sigma_s$ , one needs only to monitor the aggregation rates  $R_{\text{agg}}(s)$  for islands of size  $s$ , by monitoring the growth of the islands over a small coverage increment,  $\delta\theta \rightarrow 0$ . This can be done by introducing a counter  $M_s(\theta)$ , which is incremented by unity each time a diffusing adatom is captured by any island of size  $s$ . In terms of  $M_s$ , one has<sup>11</sup>

$$R_{\text{agg}}(s) \approx [M_s(\theta + \delta\theta) - M_s(\theta)] / (L^2 \delta\theta), \quad \text{as } \delta\theta \rightarrow 0 \quad (7)$$

for a lattice of  $L^2$  sites. Then, one has  $\sigma_s = R_{\text{agg}}(s)/(h N_1 N_s)$ , where  $N_1$  and  $N_s$  are obtained in the same simulations. The problem with this approach is that convergence of the results as  $\delta\theta \rightarrow 0$  is slow, so one needs an intensive computer effort to obtain acceptable statistics. It is much more efficient to monitor aggregation rates for ‘‘frozen’’ island distributions (i.e., without actually incrementing the island sizes), under continued deposition.<sup>11</sup> This is the general approach we take below. Quantities are typically averaged over hundreds to thousands of runs.

In the simulations, we can also monitor the complete history of every deposited atom, under continued deposition. In this way, we can assess the probability that the atom is captured by a specific island as a function of the location where it was deposited. These analyses are instructive for elucidating the stochastic nature of diffusion-mediated capture.

#### V. RESULTS FOR THE ISLAND SIZE DEPENDENCE OF CAPTURE

Figure 2 compares the form of the calculated  $\sigma_s/\sigma_{\text{av}}$  versus  $s/s_{\text{av}}$  for two distinct experimental distributions of Ag

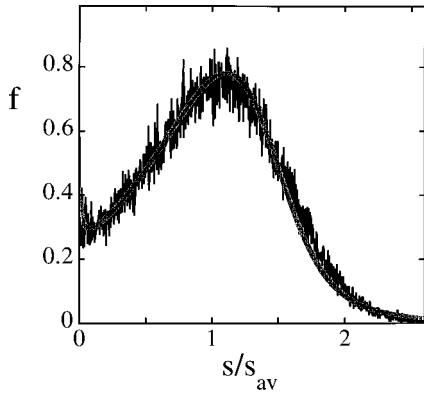


FIG. 3. Scaled island size distribution at 0.2 ML, from simulations of irreversible nucleation and growth of square islands, using  $h/F=10^9$  (black line). The gray line was obtained from numerical integration of Eq. (5), using an analytic fit of the simulation data for  $C$  in Fig. 2, and  $\bar{\omega}\approx 0.87$ .

islands on Ag(100), and for our canonical model of irreversible nucleation and growth of square islands. Experimental and model results are entirely consistent. In both cases, one finds a weak ‘‘plateau’’ in the capture numbers below  $s \approx s_{av}$ , followed by a quasilinear increase of  $\sigma_s$  with increasing  $s$ , for larger islands. These results are consistent with the form of the island size distribution,<sup>4,7,13</sup> based on relation (5) and an effective value of  $\bar{\omega}\approx 0.87$ ; see Fig. 3. Simulations also show that the scaling functions  $C$  and  $f$  are indeed independent of  $\theta$  in the range of coverages of interest here. For comparison with the above results for  $\sigma_s$  versus  $s$ , in Appendix A we present corresponding results for various special island distributions.

In addition, for both experiment and our canonical model, we obtained the ‘‘direct’’ capture numbers  $\Omega_s$  for islands of size  $s$ . These are shown in Fig. 4. The data can be fitted with the form  $\Omega_s/\Omega_{av}\approx(0.8\pm 0.02)(s/s_{av})+(0.2\pm 0.02)(s/s_{av})^{1/2}$ , which includes island area ( $\propto s$ ) and perimeter ( $\propto s^{1/2}$ ) contributions to direct capture (here  $\Omega_{av}=\sum_{s>1}\Omega_s N_s/N_{av}$ ).

## VI. GEOMETRIC PICTURE OF ADATOM CAPTURE

Here we develop a geometric picture of adatom capture which elucidates the dramatic influence of the local environment of the islands; see also Appendix B. One starts by

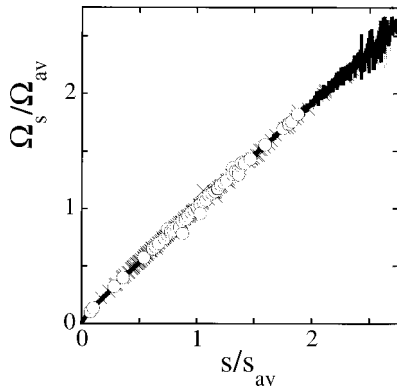


FIG. 4. Island size dependence of  $\Omega_s/\Omega_{av}$ . Lines and symbols were chosen as in Fig. 2.

constructing suitable partitions or tessellations of the entire surface into cells which surround each island. The basic expectation is that each island primarily captures adatoms deposited in its own cell or ‘‘capture zone.’’ So diffusion-mediated capture rates should be at least roughly in proportion to the areas of the part of these cells which is not covered by the island. To quantify this approach, we let  $A_s$  denote the mean area of the cells for islands of size  $s$ , and  $\tilde{A}_s=A_s-s$  denote the mean *uncovered* area (both measured in units of lattice sites). The uncovered cell area  $\tilde{A}_{av}$ , averaged over all islands, then satisfies

$$\tilde{A}_{av}=\sum_{s>1}(A_s-s)N_s/N_{av}\approx(1-\theta)/N_{av}, \quad (8)$$

since  $\sum_{s>1}A_s N_s=1$  (the tessellation covers the surface), and  $\sum_{s>1}sN_s\approx\theta$  for typical  $N_1\ll N_{av}$ . Below, after  $\tilde{A}_s$ , we indicate the corresponding tessellation in parentheses.

### A. Voronoi cells

The simplest and most conventional tessellation is a Voronoi construction based on the positions of the centers (of mass) of the islands. The construction is straightforward: for each island, the Voronoi cell (VC) is the convex polygonal region defined by the intersection of the perpendicular bisecting lines to the lines joining the center of the island to the centers of its nearest-neighbor islands.<sup>14</sup> Points within a Voronoi cell are thus closer to the center of the associated island than to those of other islands. For previous applications to surface deposition, see Refs. 10–12 and 15. The Voronoi tessellation for the experimental Ag-island distribution in Fig. 5(a) is shown in Fig. 5(b). Typically, one finds that larger islands also have larger Voronoi cells. Figure 6(a) shows that the variation of  $\tilde{A}_s(\text{VC})$  with  $s$  is similar to the variation of the capture numbers  $\sigma_s$ ; cf. Fig. 2. Differences between  $\sigma_s$  and  $\tilde{A}_s(\text{VC})$  are more pronounced for smaller islands, a feature that we elucidate below.

### B. Edge cells

It is reasonable to speculate that a Voronoi-type tessellation based on the edges of the islands, rather than on their centers, would more naturally reflect diffusion-mediated adatom capture. Each cell of such a tessellation, called here an edge cell (EC), contains the points on the surface which are closer to the edge of the associated island than to the edges of other islands. Figure 5(c) shows EC’s for the experimental distribution in Fig. 5(a). The greatest differences between EC and VC areas occurs when neighboring islands have very different sizes. Simple inspection reveals that small islands which are close neighbors of large islands have significantly larger VC’s relative to EC’s; see the diagram in Fig. 7. (Nearby large islands have correspondingly smaller VC’s relative to EC’s.) Figure 6(b) shows that the island size dependence of the EC areas,  $\tilde{A}_s(\text{EC})$ , for islands of size  $s$ , essentially recover the behavior of the  $\sigma_s$ ! In fact, we find that for our canonical model, one has  $\sigma_s/\sigma_{av}=\alpha[\tilde{A}_s(\text{EC})/\tilde{A}_{av}]+ \beta$ , with  $\alpha=1.0\pm 0.1$  and  $\beta=0.0\pm 0.1$ .

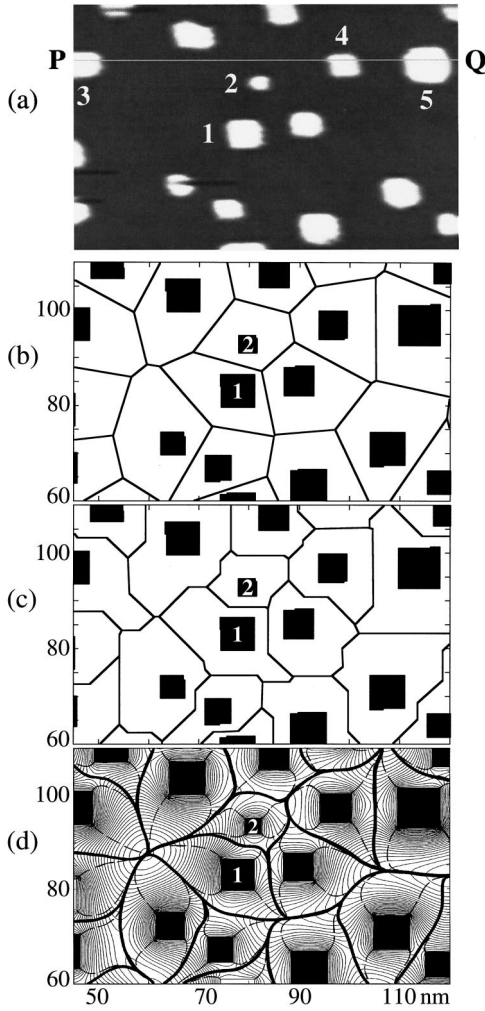


FIG. 5. (a)  $75 \times 50$ -nm<sup>2</sup> STM image (taken 42 min after deposition) of a small portion of a Ag island distribution obtained at 295 K, with  $F = 1.2 \times 10^{-2}$  ML/s and  $\theta \approx 0.12$  ML. (b) VC's, (c) EC's, and (d) DC's (thick solid lines) and contours of  $N_1$  (thin solid lines) for the island distribution in (a). The dashed lines inside each DC bound subcells for individual edge capture.

### C. Diffusion cells

Of course, neither VC's nor EC's can precisely describe adatom capture, being purely geometric constructions. However, an *exact* description can be obtained from the solution of the steady-state diffusion equation (see also Appendix C and Ref. 12)

$$\partial N_1(\mathbf{r}, t) / \partial t \approx F + D \nabla^2 N_1(\mathbf{r}, t) \approx 0, \quad (9)$$

for the density  $N_1(\mathbf{r}, t)$ , at position  $\mathbf{r}$  and time  $t$ , of deposited adatoms which diffuse to and are irreversibly captured at island edges. We thus set  $N_1 = 0$  at island edges. In Eq. (9),  $D \propto h$  is the adatom diffusion coefficient. We use a continuum formalism since discrete lattice effects are negligible for sufficiently large island sizes and separations, as applies here. Given the solution of Eq. (9) for a specific island distribution, one assigns each point on the surface to a specific island by following the lines of diffusive flux from that point to an island. The result is a tessellation of the surface into what we call diffusion cells (DC's), across the boundaries of which there is no (net) diffusive flux. Integration of Eq. (9)

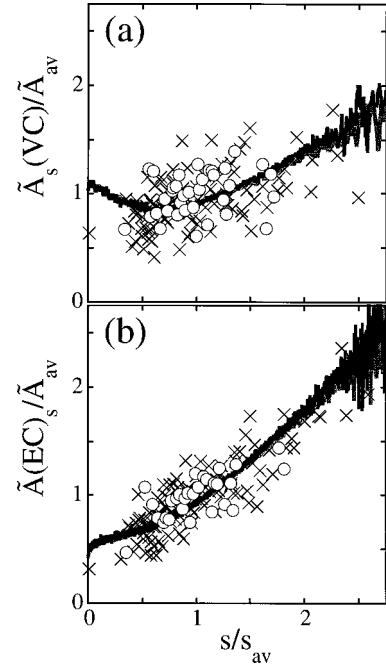


FIG. 6. Island size dependence of (a)  $\tilde{A}_s(\text{VC})/\tilde{A}_{\text{av}}$  and (b)  $\tilde{A}_s(\text{EC})/\tilde{A}_{\text{av}}$ , for square-island distributions obtained from simulations (gray lines, color coded as in Fig. 2), and from experiment (symbols chosen as in Fig. 2).

over the DC for a specific island, and application of Gauss' theorem, show that its area is indeed in *exact proportion* to the capture rates for aggregation with that island. Explicitly, one has

$$\begin{aligned} 0 &\approx \iint_{\text{DC}} (F + D \nabla^2 N_1) d\tilde{A}_{\text{DC}} \\ &= F \tilde{A}_{\text{DC}} - D \int_{\text{perimeter}} (\nabla N_1 \cdot \mathbf{n}) dl, \end{aligned} \quad (10)$$

where  $\tilde{A}_{\text{DC}}$  is the uncovered area of the DC, and  $\mathbf{n}$  the unit vector normal to the island perimeter. Thus, using Eq. (10) and the steady-state relation for  $N_1$ , one obtains for the capture number  $\sigma_{\text{DC}}$  of the island of interest the result

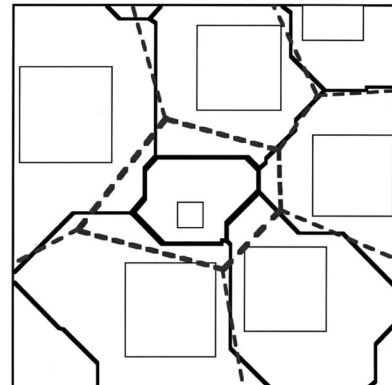


FIG. 7. Schematic of a configuration where nearby islands have very different size, producing significantly different VC- and EC-cell distributions especially for the smaller islands.

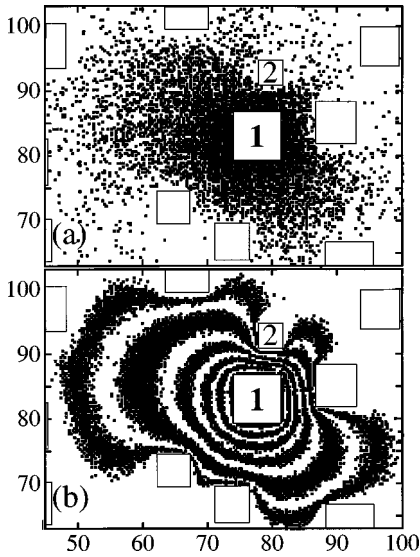


FIG. 8. Simulation results for capture by island 1 in Fig. 5(a). (a) “Fuzzy” capture sets: Dots are the landing sites of adatoms captured by the island during a certain time interval. (b) Spatial distribution of adatom capture probabilities. Successive black-and-white bands (away from the island) distinguish sites which differ in  $P$  by 0.1, except for the last two pairs of bands which differ by 0.05 and 0.025, respectively. Axis labels are in nm.

$$\begin{aligned} \sigma_{\text{DC}} &= (1/N_1) \int_{\text{perimeter}} (\nabla N_1 \cdot \mathbf{n}) dl \\ &= (1 - \theta)^{-1} \sigma_{\text{av}} N_{\text{av}} \tilde{A}_{\text{DC}} = \sigma_{\text{av}} \tilde{A}_{\text{DC}} / \tilde{A}_{\text{av}}. \end{aligned} \quad (11)$$

The DC’s for the experimental island distribution in Fig. 5(a) are shown in Fig. 5(d). It is possible to decompose the DC’s further into subcells corresponding to capture by individual island edges, as illustrated in Fig. 5(d), so that flux lines in each subcell flow to the appropriate edge.<sup>12</sup> The areas of these subcells are in *exact proportion* to the capture numbers for individual edges.

As noted in Sec. III, the variation of  $\sigma_s$  with  $s$  is *qualitatively distinct* from that predicted by MF theories,<sup>9,10</sup> where the environment of islands is assumed to be independent of their size. To elucidate the exact form, we note that the first islands which nucleate tend to have larger “capture areas,” i.e., larger surrounding island-free areas, than newer islands, and consequently grow larger. (See Appendix D for further details on island age issues.) The weak “plateau” in  $\sigma_s$  for  $s < s_{\text{av}}$  then arises as newer islands grow and effectively transfer (smaller) capture areas from smaller to larger island sizes.

## VII. STOCHASTIC ASPECTS OF ADATOM CAPTURE

It is important to emphasize that, since adatom diffusion is stochastic in nature, atoms deposited within a DC are *not* definitely captured by the associated island. That is, the probability that an atom is captured by an island is not unity inside its DC and zero outside; rather it decreases smoothly to zero away from the island edge.<sup>12</sup> This feature is illustrated with simulation results in Figs. 8 and 9, for two Ag islands (labeled “1” and “2” in Fig. 5) which have distinct local environments, and thus different capture rates. In Figs.

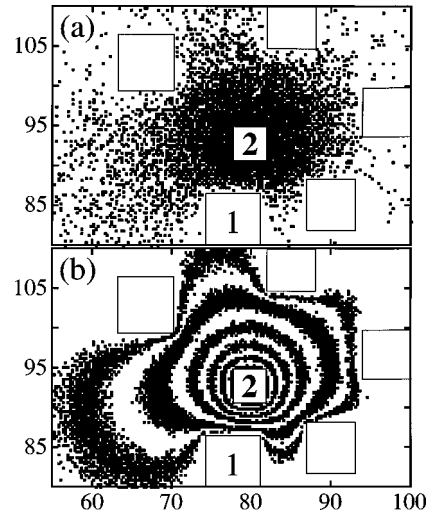


FIG. 9. The same as Fig. 8 for island 2 in Fig. 5(a).

8(a) and 9(a), dots are assigned to an island if atoms that landed on those sites, during a certain time interval, were captured by that island. Note the *fuzziness* of these sets of dots, especially far from the island.

For a more precise characterization, one can consider the probability  $P$  that a diffusing adatom is captured by a specific island, for various starting locations of the adatoms on the surface. The above simulations can also be used to determine  $P$ , and such results are shown in Figs. 8(b) and 9(b). It is appropriate to note that an analytic formalism can also be developed to determine the  $P$ ’s. Specifically, in the continuum limit,  $P$  satisfies the Laplace equation  $\nabla^2 P = 0$ , with  $P = 1$  at the perimeter of the specified island, and  $P = 0$  at the perimeter of all other islands.<sup>16</sup> Contours of  $P$  from the numerical solution of this equation, shown in Fig. 10 for the two islands selected above, are in perfect agreement with simulation results. Both analyses reveal a nontrivial spatial

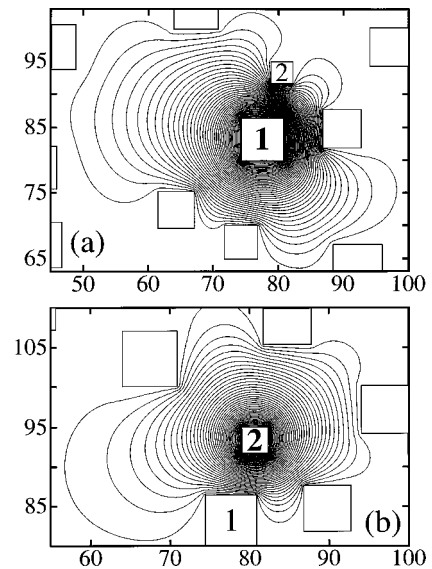


FIG. 10. Contours of  $P$  for (a) island 1, and (b) island 2 in Fig. 5(a), from the numerical solution of the Laplace equation.  $P = 1$  at the edge of the specific island, and  $P = 0$  at the edge of all other islands.  $P$  decreases by 0.025 for each successive contour line away from the edge of the islands. Axis labels are in nm.

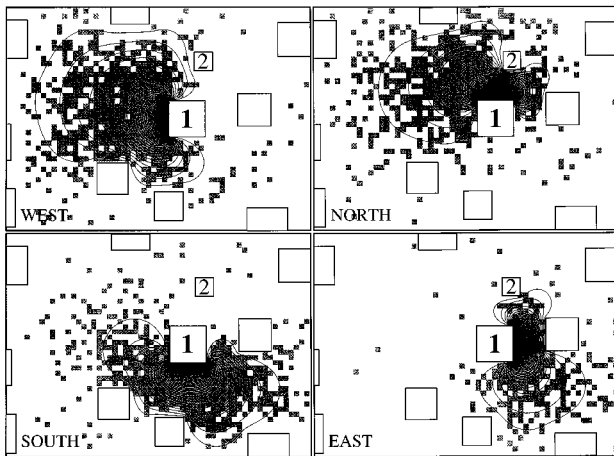


FIG. 11. Simulation (dots) and steady-state diffusion equation (contour lines) results for  $P_{\text{edge}}$ , for island 1 in Fig. 5(a). In each frame,  $P_{\text{edge}}=1$  on the specific (north, south, east or west) edge of the island, and  $P_{\text{edge}}=0$  on all other edges of this and other islands.

variation of capture probabilities, with the complex structure of the  $P$  contours reflecting the local arrangement of nearby islands.

One can also consider probabilities  $P_{\text{edge}}$  for capture at a specific island edge. Analytically, one has  $\nabla^2 P_{\text{edge}}=0$ , with  $P_{\text{edge}}=1$  just on that edge. Figures 11 and 12 compare contours of  $P_{\text{edge}}$  with the corresponding fuzzy simulation sets of the two islands selected above. Clearly, edges facing emptier surrounding areas capture more diffusing adatoms. We note that information on  $P_{\text{edge}}$  is especially useful in studies where significant kinetic limitations exist for atoms at island edges to diffuse around the corners between edges, as this process controls equilibration of the island shape.<sup>17</sup>

## VIII. SIMILAR CAPTURE BEHAVIOR IN OTHER SYSTEMS

### A. Capture of Cu atoms by Co islands on Ru(0001)

The dependence of Cu adatom capture on the size of Co islands on Ru(0001) was recently examined with STM,<sup>12</sup> in what was the first experiment tailored to address this issue. In the experiment, a nonrandom distribution of near-hexagonal islands of Co on Ru(0001) is first produced by Co

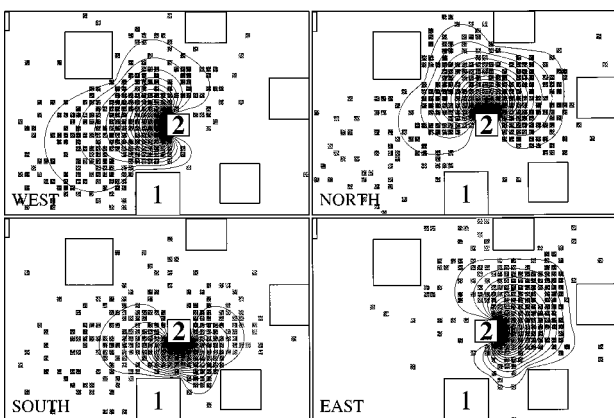


FIG. 12. The same as Fig. 11 for island 2 in Fig. 5(a).

deposition at 50 °C and subsequent flash annealing to 350 °C. This is followed by exposure to Cu at room temperature. STM contrast between Cu and Co regions reveals that most Cu attached to the perimeter of the Co islands, forming ‘‘rings.’’ Due to limited restructuring, the Cu rings around the Co islands have nonuniform widths, indicating larger growth rates in directions facing wider empty regions.

From the amount of Cu in the rings, we measured  $\sigma_s$  versus  $s$ . Results in Ref. 12 show the same basic form as that in Fig. 2, i.e., a plateau below  $s \approx s_{\text{av}}$ , followed by a quasi-linear increase in  $\sigma_s$  with  $s$ , for large  $s$ . This form is also reproduced by simulations tailored for this system.<sup>12</sup> Results for overall and edge-specific capture probabilities (analogous to Figs. 8–12) are completely consistent with the observed anisotropic structure of the Cu rings around the Co islands.<sup>12</sup>

### B. Growth of pits on Si(001) surfaces etched with O<sub>2</sub>

Low-energy electron microscopy (LEEM) studies of high-temperature etching of nominally flat Si(001) terraces with molecular oxygen have allowed real-time, *in situ* measurements of the environment dependence of the growth rates of two-dimensional etch pits.<sup>18</sup> This growth is controlled by diffusion and aggregation of vacancies, which are created at random locations during etching, analogous to the random deposition and subsequent diffusion of adatoms in the above growth studies.

As for metal islands, one finds large variations in pit growth rates, pits with fewer neighbors growing faster. Variation in pit shapes, evident in the data,<sup>18</sup> reflects the direction dependence of vacancy capture, combined with limited diffusion at the edge of large pits. These observations suggest that pit growth is dominated by the rate at which diffusing vacancies arrive at the edge of individual pits. Indeed, data for the pit sizes versus time, monitored with LEEM at video rates, show that the pit growth rates directly reflect their local environment.<sup>18</sup> Simulation results for a distribution of pits and steps matching experiment are in excellent agreement with the measured growth rates and instantaneous island sizes. Identical results are obtained based on the DC areas.<sup>18</sup>

## IX. CONCLUSIONS

In summary, we have presented a comprehensive analysis of the island size and environment dependence of the capture of Ag adatoms by arrays of near-square Ag islands during deposition on Ag(100) at room temperature. Results show that such diffusion-mediated capture reflects strong correlation between the size of an island and the area of the empty region surrounding the island. In simple geometric terms, the capture rate is accurately described by the area of cells in a Voronoi-type tessellation based on the edges of islands, rather than on their centers of mass. This detailed characterization of adatom capture is crucial for an understanding of the form of the island size distribution, as well as for assessing the growth of individual islands.

The above presentation does not completely explain the precise form selected for the size dependence of adatom capture for irreversible formation of compact islands. Our current efforts in developing a theoretical framework to clarify this issue indicate that this form depends crucially on the

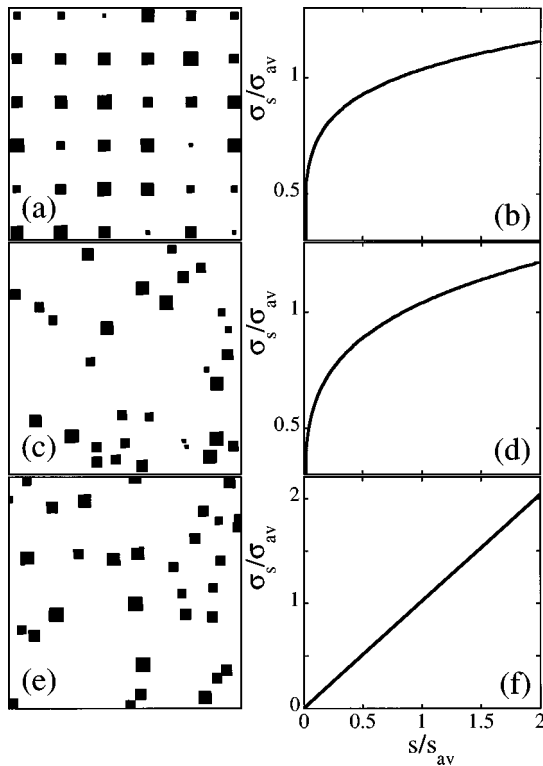


FIG. 13. Special island distributions and their capture numbers. (a) and (b) Periodically distributed islands, random island sizes. (b) and (c) Randomly distributed islands, random island sizes. (e) and (f) Randomly distributed islands, sizes determined during growth. Statistics were obtained on  $1000 \times 1000$  site lattices.

initial stages of island nucleation. Also, it is known that the form of the island size distribution is sensitive to the details of island shape (including ramification<sup>19</sup> or anisotropy<sup>20</sup>), to significant diffusion of dimers and other small clusters,<sup>21</sup> to the onset of reversibility in island formation,<sup>4,22</sup> and to anisotropy in terrace diffusion.<sup>6,23</sup> Thus we are examining the extent to which this sensitivity reflects underlying changes in the form of the size dependence of adatom capture.

#### ACKNOWLEDGMENTS

This work was supported by the Office of Basic Energy Sciences, Division of Materials Sciences, of the U.S. DOE, and performed in part at Sandia National Laboratories (M.C.B.). Sandia is a multiprogram laboratory operated for the U.S. DOE by Sandia Corporation, a Lockheed Martin Company, under Contract No. DE-AC04-94AL85000. This work was also supported by NSF Grant No. CHE-9700592 and IPRT (C.R.S., C.J.J., P.A.T., J.W.E.), and performed at Ames Laboratory. Ames Laboratory is operated for the U.S. DOE by Iowa State University under Contract No. W-7405-Eng-82.

#### APPENDIX A: ADATOM CAPTURE BY SPECIAL ISLAND DISTRIBUTIONS

It is instructive to consider adatom capture by arrays of islands with specified size and separation distributions. We focus on the behavior of the  $\sigma_s$  for three cases:

- (i) *Periodically distributed islands; random island sizes.*

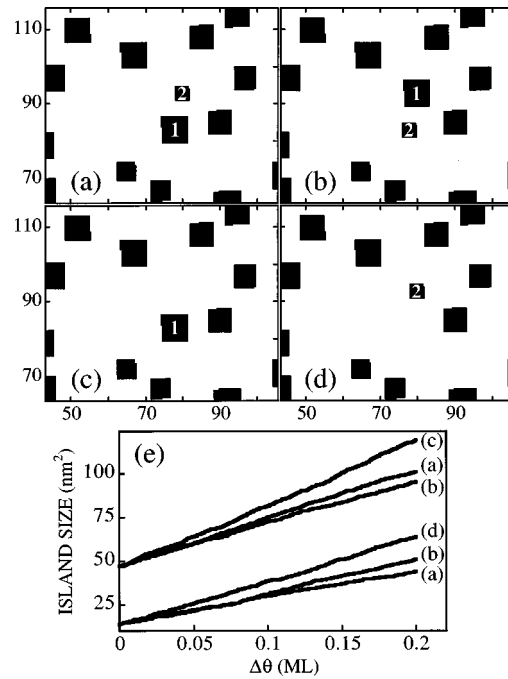


FIG. 14. Simulation results for the growth rates of islands 1 and 2 in Fig. 5(a), for (a) the original experimental distribution, (b) when the island positions are switched, and (c) and (d) when one of the islands is removed. In (e),  $\Delta\theta$  is the additional coverage. In (a)–(d), axes labels are in nm.

Figure 13(a) shows a configuration of islands arranged in a square array (so VC's are equal for all islands), with sizes, and thus EC areas, selected randomly, subject to an upper cutoff to avoid coalescence. That is, the environment of the islands does not depend on their size. One therefore recovers MF-like behavior<sup>5</sup> for the  $\sigma_s$ ; see Fig. 13(b).

(ii) *Randomly distributed islands; random island sizes.* Figure 13(c) shows a configuration of islands placed at random positions, with sizes also selected randomly subject to an upper cutoff as in (i) (which here does not prevent coalescence as clustering typically occurs in randomly selected positions; we treat overlapping islands as individual islands). As in (i),  $\sigma_s$  are weakly dependent on  $s$ ; see Fig. 13(d). Differences in the form of the  $\sigma_s$  relative to (i) presumably reflect differences in the short-range features of the island distribution.

(iii) *Randomly distributed islands; sizes determined during growth.* Here we let islands grow during deposition, from randomly placed few-atom seeds; see Fig. 13(e). The resulting island size distribution is nonrandom, since seeds with larger empty surrounding areas grow larger in direct proportion to these areas. In fact, like the EC areas, here  $\sigma_s$  increase linearly with island size; see Fig. 13(f). A weak plateau, as in Fig. 2, does not develop for small sizes due to the lack of nucleation of new islands.<sup>11</sup>

#### APPENDIX B: TAILORED STUDIES OF THE ENVIRONMENTAL DEPENDENCE OF ADATOM CAPTURE

To assess the environment dependence of the island growth rates directly, we monitored the growth of islands 1 and 2 in Fig. 5(a) during deposition of an additional 0.2 ML,

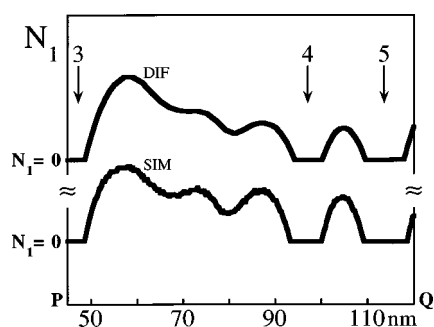


FIG. 15. Contour of  $N_1$  for positions along the line between  $P$  and  $Q$  in Fig. 5(a). Shown are results from simulations (SIM) and from the numerical solution of the steady-state diffusion equation (DIF).

and then examined the effect of simple modifications in the surroundings of the islands on their growth rates. Figure 14(a) shows that, in the original distribution, island 1 grows  $\sim 1.8$  times faster than island 2, consistent with the results in Fig. 2, namely,  $\sigma_{\dots,1} / \sigma_{\dots,2} \approx 2$ . Switching the island positions, as in Fig. 14(b), increases the growth rate of island 2, but lowers that of island 1. Capture rates increase significantly for both islands when the other is absent, as in Figs. 14(c) and 14(d).

#### APPENDIX C: STEADY-STATE BEHAVIOR OF THE ADATOM DENSITY

We compared the steady-state form of  $N_1(\mathbf{r})$  obtained from the numerical solution of the diffusion equation in Eq. (9) with the corresponding behavior obtained directly from

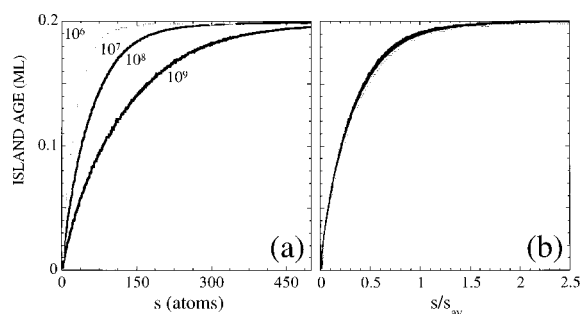


FIG. 16. (a) The size dependence of the island age,  $\tau_s$ , from simulations of irreversible nucleation and growth of square islands. Data are for  $h/F = 10^6 - 10^9$  and  $\theta = 0.2$  ML. (b) Scaling of  $\tau_s$  with  $s/s_{av}$ , where  $s_{av} \sim 0.4(h/F)^{1/3}$  (in units of lattice sites). Specifically,  $s_{av} \approx 40, 84, 180,$  and  $390$ , for  $h/F = 10^6, 10^7, 10^8,$  and  $10^9$ , respectively.

the simulations (under continued deposition for improved statistics). In the simulations, an array monitors the probability of finding a diffusing adatom at any site on the surface. Figure 15 shows a cross section of  $N_1(\mathbf{r})$  obtained for the Ag-island distribution in Fig. 5(a). Results from simulations and the diffusion equation analysis agree in detail.

#### APPENDIX D: ISLAND AGE VERSUS SIZE

For irreversible nucleation and growth of square islands, we recorded the age of every island, and calculated the average  $\tau_s$  for each island size  $s$ . Simulation results in Fig. 16, for deposition of 0.2 ML, show that, on average, smaller islands (with  $s < s_{av}$ ) are actually older (due to their smaller capture) than one might anticipate.

<sup>1</sup>C. Günther, S. Günther, E. Kopatzki, R. Q. Hwang, J. Schröder, J. Vrijmoeth, and R. J. Behm, *Ber. Bunsenges. Phys. Chem.* **97**, 522 (1993); R. Q. Hwang and M. C. Bartelt, *Chem. Rev.* **97**, 1063 (1997); G. Rosenfeld, B. Poelsema, and G. Comsa, in *Growth and Properties of Ultrathin Epitaxial Layers*, edited by D. A. King and D. P. Woodruff, *Chemical Physics of Solid Surfaces*, Vol. 8 (Elsevier, Amsterdam, 1998), Chap. 3; H. Brune, *Surf. Sci. Rep.* **31**, 121 (1998).

<sup>2</sup>M. Smoluchowski, *Phys. Z.* **17**, 557 (1916); **17**, 585 (1916).

<sup>3</sup>*Kinetics of Aggregation and Gelation*, edited by F. Family and D. P. Landau (North-Holland, Amsterdam, 1984).

<sup>4</sup>L. Bardotti, C. R. Stoldt, C. J. Jenks, M. C. Bartelt, J. W. Evans, and P. A. Thiel, *Phys. Rev. B* **57**, 12 544 (1998); L. Bardotti, M. C. Bartelt, C. J. Jenks, C. R. Stoldt, J.-M. Wen, C.-M. Zhang, P. A. Thiel, and J. W. Evans, *Langmuir* **14**, 1487 (1998); C.-M. Zhang, M. C. Bartelt, J.-M. Wen, C. J. Jenks, J. W. Evans, and P. A. Thiel, *Surf. Sci.* **406**, 178 (1998).

<sup>5</sup>A. F. Voter, *Proc. SPIE* **821**, 6819 (1986); B. D. Yu and M. Scheffler, *Phys. Rev. B* **55**, 13 916 (1997).

<sup>6</sup>M. C. Bartelt and J. W. Evans, *Phys. Rev. B* **46**, 12 675 (1992); M. C. Bartelt, M. C. Tringides, and J. W. Evans, *ibid.* **47**, 13 891 (1993); and in *Evolution of Surface and Thin Film Microstructure*, edited by H. A. Atwater, E. Chason, M. H. Grabow, and M. G. Lagally, *MRS Symposia Proceedings No. 280* (Materials Research Society, Pittsburgh, 1993) p. 363; J. W. Evans and M. C.

Bartelt, *Surf. Sci.* **284**, L437 (1993); *J. Vac. Sci. Technol. A* **12**, 1200 (1994).

<sup>7</sup>M. C. Bartelt and J. W. Evans, *Surf. Sci.* **298**, 421 (1993); and in *Common Themes and Mechanisms of Epitaxial Growth*, edited by P. Fuoss, J. Tsao, D. W. Kisker, A. Zangwill, and T. Kuech, *MRS Symposia Proceedings No. 312* (Materials Research Society, Pittsburgh, 1993) p. 255; J. W. Evans and M. C. Bartelt, in *Morphological Organization in Epitaxial Growth and Removal*, edited by Z. Zhang and M. G. Lagally (World Scientific, Singapore, 1998).

<sup>8</sup>H. Brune, H. Röder, C. Boragno, and K. Kern, *Phys. Rev. Lett.* **73**, 1955 (1994); M. Bott, M. Hohage, M. Morgenstern, T. Michely, and G. Comsa, *ibid.* **76**, 1304 (1996).

<sup>9</sup>S. Stoyanov, *Curr. Top. Mater. Sci.* **3**, 421 (1979); S. Stoyanov and D. Kashchiev, *ibid.* **7**, 69 (1981); G. S. Bales and D. C. Chrzan, *Phys. Rev. B* **50**, 6057 (1994).

<sup>10</sup>J. A. Venables and D. J. Ball, *Proc. R. Soc. London, Ser. A* **322**, 331 (1971); J. A. Venables, *Philos. Mag.* **27**, 697 (1973).

<sup>11</sup>M. C. Bartelt and J. W. Evans, *Phys. Rev. B* **54**, R17 359 (1996); and in *Structure and Evolution of Surfaces*, edited by R. C. Cammarata, E. H. Chason, T. L. Einstein, and E. D. Williams, *MRS Symposia Proceedings No. 440* (Materials Research Society, Pittsburgh, 1997), p. 247.

<sup>12</sup>M. C. Bartelt, A. K. Schmid, J. W. Evans, and R. Q. Hwang, *Phys. Rev. Lett.* **81**, 1901 (1998); M. C. Bartelt, J. W. Evans, A.

- K. Schmid, and R. Q. Hwang, in *Mechanisms and Principles of Epitaxial Growth in Metallic Systems*, edited by L. T. Wille, C. P. Burmester, K. Terakura, G. Comsa, and E. D. Williams, MRS Symposia Proceedings No. 528 (Materials Research Society, Pittsburgh, 1998).
- <sup>13</sup>C. R. Stoldt, A. M. Cadilhe, M. C. Bartelt, C. J. Jenks, P. A. Thiel, and J. W. Evans, *Prog. Surf. Sci.* (to be published).
- <sup>14</sup>See, e.g., F. P. Preparata and M. I. Shamos, *Computational Geometry: An Introduction* (Springer-Verlag, Berlin, 1985).
- <sup>15</sup>P. A. Mulheran and J. A. Blackman, *Philos. Mag. Lett.* **72**, 55 (1995); *Phys. Rev. B* **53**, 10 261 (1996).
- <sup>16</sup>J. W. Evans, *Phys. Rev. A* **40**, 2868 (1989).
- <sup>17</sup>M. C. Bartelt and J. W. Evans, *Surf. Sci.* **314**, L829 (1994); H. Röder, K. Bromann, H. Brune, and K. Kern, *Phys. Rev. Lett.* **74**, 3217 (1995); M. Hohage, M. Bott, M. Morgenstern, Z. Zhang, T. Michely, and G. Comsa, *ibid.* **76**, 2366 (1996); H. Brune, H. Holger, K. Bromann, K. Kern, J. Jacobsen, P. Stolze, K. Jacobsen, and J. Nørskov, *Surf. Sci.* **349**, L115 (1996).
- <sup>18</sup>J. B. Hannon, M. C. Bartelt, N. C. Bartelt, and G. L. Kellogg, *Phys. Rev. Lett.* **81**, 4676 (1998); *Surf. Rev. Lett.* (to be published).
- <sup>19</sup>J. G. Amar and F. Family, in *Fractal Aspects of Materials*, edited by F. Family, P. Meakin, B. Sapoval, and R. Wool, MRS Symposia Proceedings No. 367 (Materials Research Society, Pittsburgh, 1995).
- <sup>20</sup>M. M. R. Evans and J. Nogami (unpublished).
- <sup>21</sup>M. C. Bartelt, S. Günther, E. Kopatzki, R. J. Behm, and J. W. Evans, *Phys. Rev. B* **53**, 4099 (1996); L. Kuipers and R. E. Palmer, *ibid.* **53**, R7646 (1996).
- <sup>22</sup>J. A. Stroschio and D. T. Pierce, *Phys. Rev. B* **49**, 8522 (1994); C. Ratsch, P. Smilauer, A. Zangwill, and D. D. Vvedensky, *Surf. Sci.* **329**, L599 (1995); J. G. Amar and F. Family, *Phys. Rev. Lett.* **74**, 2066 (1995).
- <sup>23</sup>T. R. Linderoth, J. J. Mortensen, K. W. Jacobsen, E. Lægsgaard, I. Stensgard, and F. Besenbacher, *Phys. Rev. Lett.* **77**, 87 (1996); J. J. Mortensen, T. R. Linderoth, K. W. Jacobsen, E. Lægsgaard, I. Stensgard, and F. Besenbacher, *Surf. Sci.* **400**, 290 (1998).